Model Predictive Charging Control of In-Vehicle Batteries for Home Energy Management Based on Vehicle State Prediction

Akira Ito, *Member, IEEE*, Akihiko Kawashima, *Member, IEEE*, Tatsuya Suzuki, *Member, IEEE*, Shinkichi Inagaki, *Member, IEEE*, Takuma Yamaguchi, and Zhuomin Zhou

***Abstract*— Thanks to recent development of reciprocal communication networks and electric power management infrastructure, an energy management system, which can automatically regulate supply-demand imbalances under conditions of the users' convenience and economy, is attracting great attention. On the other hand, finding of new usage of the batteries employed in electric vehicles and plug-in hybrid vehicles is recognized as one of key issues to realize the sustainable society. In addition, development of vehicle to X technology enables us to use the electric power of in-vehicle batteries for various purposes. Based on these backgrounds, this paper presents an integrated strategy for charging control of in-vehicle batteries that optimizes the charge/discharge of in-vehicle batteries in a receding horizon manner exploiting the predicted information on home power load and future vehicle state in the household. The prediction algorithm of future vehicle state is developed based on semi-Markov model and dynamic programming. In addition, it can also be implemented in receding horizon manner, i.e., the predicted vehicle state is updated at every control cycle based on the new observation. Thus, the harmonious combination of stochastic modeling/prediction and MPC in real-time home energy management system is one of the main contributions of this paper. Effectiveness of the proposed charging control is demonstrated by using an experimental testbed.**

***Index Terms*— Dynamic programming (DP), home energy management system (HEMS), in-vehicle battery, model predictive control (MPC), vehicle state prediction.**

I. Introduction

SMART grid infrastructures [1] have attracted substantial interest for use as highly effective electric power management systems working in tandem with recently developed reciprocal communication networks. One of the most important considerations for a smart grid system is maximum utilization of renewable power sources such as photovoltaics (PVs) and wind-powered generators, which is beneficial in terms of economy and sustainability.

To obtain supply-demand balance while using renewable energy sources, a dynamic pricing (DP) strategy that aims to influence consumer demand to bring it more in line with supply has been proposed [2], [3]. The success of the DP strategy, however, strongly depends on the actual responses of customers to time-varying prices [4]. As can be easily imagined, it is generally inconvenient and impractical to have customers continuously keep being aware of prices. Therefore, an energy management system, which can automatically regulate supply–demand imbalances under conditions of the users' convenience and economy, is required.

From these perspectives, the importance of home energy management system (HEMS) is growing, because it has a potential to meet the requirement of supply–demand balance automatically with considering the customer's demand explicitly. Two basic techniques have been used within the framework of the HEMS to achieve automatic supply–demand balance in household. The first technique is a load-side control. This technique focuses on operational or power consumption flexibility for household appliances and attempts to schedule appliance operation to avoid consumer inconvenience [5], [6]. This method is appropriate for commercial facilities that have well-regulated power demands. The second technique is a supply-side control. This technique focuses on scheduling of power storage such as batteries and heat pumps. Storage enables the maximum use of renewable energy and results in low energy cost, and provides power according to consumer demand [7], [8]. This technique is appropriate for homes wherein power demand tends to vary. However, typical storage systems such as batteries, particularly ones employed in the HEMS, have their own challenges because of the difficulty in obtaining the optimal tradeoff between cost and size of the storage system.

To address these concerns, the batteries employed in electric vehicles (EVs) and plug-in hybrid vehicles (PHVs) have been proposed to serve the dual purpose of transportation and home electric power storage [9]–[11]. This is also motivated by the grave concern of finding new usage of the batteries

Manuscript received July 2, 2016; revised October 3, 2016 and January 14, 2017; accepted January 24, 2017. Date of publication February 23, 2017; date of current version December 14, 2017. Manuscript received in final form January 29, 2017. This work was supported by JST, CREST. Recommended by Associate Editor S. Di Cairano.

A. Ito and Z. Zhou are with the Engineering Research and Development Center, DENSO CORPORATION, Kariya 448-8661, Japan (e-mail: akira_ito@denso.co.jp; takubin_shu@denso.co.jp).

A. Kawashima, S. Inagaki, and T. Yamaguchi are with the Department of Mechanical Science and Engineering, Nagoya University, Nagoya 464-8603, Japan (e-mail: a_kawashima@nuem.nagoya-u.ac.jp; inagaki@nuem.nagoya-u.ac.jp; t_yamaguchi@nuem.nagoyau.ac.jp).

T. Suzuki is with the Department of Mechanical Science and Engineering, Nagoya University, Nagoya, Japan, and also with JST, CREST, Tokyo 102-0076, Japan (e-mail: t_suzuki@nuem.nagoya-u.ac.jp).

Color versions of one or more of the figures in this paper are available online at http://ieeexplore.ieee.org.

Digital Object Identifier 10.1109/TCST.2017.2664727

employed in EVs and PHVs in automobile society [12], [13]. Although there have been lots of works investigating how to embed the EVs in the HEMS [14]–[16], the problem how to deal with the dual purpose at each household has not been clearly addressed yet. In previous studies [17], [18], for example, the start time of battery charge or discharge was scheduled according to the preset profile for departure and arrival times of the vehicle. However, owing to the dual purpose, the HEMS that exploits in-vehicle batteries must plan the charge and discharge schedule based on the predicted future vehicle state (i.e., used for transportation or not) that reflects the customer demand. This necessitates the explicit combination of the real-time optimization and the prediction of the future vehicle state in the design of the HEMS.

As for the prediction strategy of the future vehicle state, there have been some works [19], [20]. These works, however, focused on the prediction of aggregated vehicle state of massive cars. In the car navigation system, although there have also been some works to predict travel time to reach the destination [21], [22], the explicit prediction of the departure time at home was not fully addressed.

Considering these backgrounds, this paper presents an HEMS which integrates a prediction of future vehicle usage and home load, optimization of the charge/discharge profile of the in-vehicle batteries employed in EVs or PHVs, and real-time execution by using model predictive control (MPC) framework. In prediction part, first of all, the home power load prediction is investigated by using autoregressive (AR) model, then, a prediction scheme for the most likely future vehicle state sequence, i.e., the profile of vehicle departure and arrival times in household, is developed. This is achieved by using dynamic programming (DP) over semi-Markov model which is designed based on statistical data of daily vehicle use [23], [24]. The HEMS optimizes the charge/discharge profile of the in-vehicle batteries under consideration of many important constraints. The optimization is formulated by using mixed integer linear programming (MILP) so as to minimize the daily home electricity cost based on predictions. In addition, the optimization is made in real time using receding horizon manner, which can improve the robustness against the prediction and/or modeling errors. The effectiveness of the proposed scheme is experimentally verified by using HEMS experimental testbed, and discussed particularly focusing on the robustness and economical benefits.

Since the proposed vehicle state prediction can be implemented in receding horizon manner, i.e., vehicle state prediction is updated at every control cycle based on the new observation, it has high compatibility with MPC. Thus, the combination of stochastic modeling/prediction and MPC, and its implementation on real-time HEMS are important contributions of this paper. The strategy of combining stochastic modeling/prediction and MPC is also found in some other application fields [25], [26], which show higher performance than the conventional control schemes.

The remaining part of this paper is organized as follows. Section II describes the formulation of the HEMS on the basis of MPC with receding horizon prediction and optimization. Section III investigates the prediction of the home power load. In Section IV, the prediction scheme of future vehicle state sequence is developed based on the statistical data of daily vehicle use and DP over semi-Markov model. Section V explains about the experimental testbed, which integrates the prediction, optimization, and implementation. Section VI provides discussions on the robustness of the proposed HEMS against the modeling and prediction error. The economic benefits are also discussed. The conclusions are made in Section VII.

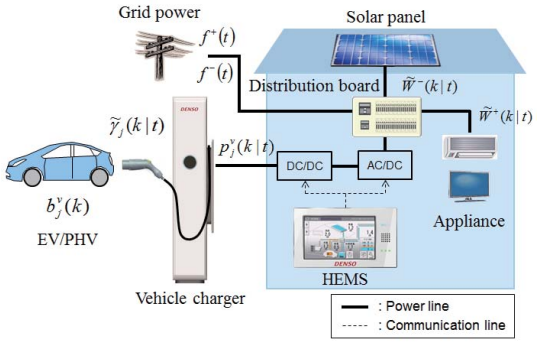

Fig. 1. Variables used for the formulation of HEMS.

II. Formulation of HEMS on the Basis of MPC

A. Definition of Variables and Parameters

As shown in Fig. 1, a household is supposed to have N EVs and PHVs in total and a PV generator. In our formulation, one day is divided by a sampling time Δt into T steps, where Δt is 30 [min] and T is 48. The definition of variables and parameters in the HEMS for $k = t, \ldots, t+T-1$ and $j = 1, \ldots, N$ are as follows.

$\tilde{W}^+(k\|t) \geq 0$	Home power load (electric power consumed in home) at time k predicted at t (W).
$\tilde{W}^-(k\|t) < 0$	Electric power generated in home at time k predicted at t (W).
$\tilde{\gamma}_j(k\|t) \in \{0,1\}$	Binary-valued vehicle state indicating whether the vehicle j is available in the HEMS at time k predicted at t, where $\tilde{\gamma}_j(k\|t) = 0$ indicates that the vehicle is connected to the home, and $\tilde{\gamma}_j(k\|t) = 1$ indicates that the vehicle is used for transportation.
$\tilde{B}_j^{\mathrm{v,cons}}(k\|t) \geq 0$	Consumed electric energy of vehicle j by driving at time k predicted at t (Wh).
$b_j^{\mathrm{v}}(k\|t) \geq 0$	Electric energy of battery of vehicle j at time k predicted at t (Wh).
$p_j^{\mathrm{v}}(k\|t)$	Charging or discharging electric power of vehicle j at time k planned at t (W), where $p_j^{\mathrm{v}}(k\|t) \geq 0$ indicates charge of the in-vehicle battery and $p_j^{\mathrm{v}}(k\|t) < 0$ indicates discharge of the in-vehicle battery.
$f^+(t) > 0$	Purchase price of electric energy at t (Yen/Wh).
$f^-(t) > 0$	Sale price of electric energy at t (Yen/Wh).

$B_j^{\mathrm{v,min}}(t) \geq 0$	Lower bound of electric energy of battery of vehicle j at t (Wh).
$B_j^{\mathrm{v,max}} > 0$	Upper bound of electric energy of battery of vehicle j (Wh).
$B_j^{\mathrm{v,init}} \geq 0$	Initial value of electric energy of battery of vehicle j (Wh).
$W_{\max} > 0$	Upper bound of electric power in household (W).
$W_{\min} < 0$	Lower bound of electric power in household (W).
$J_{\max} > 0$	Upper bound of total electric energy in one day in household (Wh).
$P_j^{\mathrm{v,char}} > 0$	Upper bound of electric power for charging the battery of vehicle j from home (W).
$P_j^{\mathrm{v,dis}} < 0$	Upper bound of electric power for discharging the battery of vehicle j to home (W).
$P^{\mathrm{standby}} \geq 0$	Standby power of power conditioner system (W).
η^{char}	Coefficient of charge.
η^{dis}	Coefficient of discharge.
η^{pv}	Coefficient of photovoltaic generation.
η^{acdc}	Coefficient of conversion between ac and dc.

In these definitions, the notation " ˜ " indicates a predicted value. The HEMS uses the predicted profiles of electric power consumed in household, $\tilde{W}^+(k|t)$ and vehicle state, $\tilde{\gamma}_j(k|t)$, $\tilde{B}_j^{\mathrm{v,cons}}(k|t)$. The profile of electric power consumed in household $\tilde{W}^+(k|t)$ is predicted based on standard AR model [27], [28]. The prediction of vehicle state $\tilde{\gamma}_j(k|t)$ is discussed in Section III. On the other hand, it is assumed that PV power generation $\tilde{W}^-(k|t)$ is known. Numerous studies have been conducted that seek to predict PV power generation [29], [30]. Results of these studies are available in this paper.

In Section II-B, the optimization problem of charge/discharge profile over one day is formulated by using these parameters and variables.

B. Formulation of the Optimization Problem

The problem of scheduling a charge/discharge profile for in-vehicle batteries to minimize the electricity costs can be formulated as an MILP. The objective function, decision variables, and constraint conditions are given by the following problem statement.

Optimization of Charge of In-Vehicle Batteries:

Given $\{\tilde{W}^+(k|t),\ \tilde{W}^-(k|t),\ \tilde{\gamma}_j(k|t),\ \tilde{B}_j^{\mathrm{v,cons}}(k|t),\ f^+(k),\ f^-(k),\ B_j^{\mathrm{v,min}}(k|t),\ B_j^{\mathrm{v,init}}\}_{k\in\{t,\ldots,t+T-1\}}$,

find $\{p_j^{\mathrm{v}}(k|t)\}_{k\in\{t,\ldots,t+T-1\}}$,

which minimize

$$Z = \sum_{k=t}^{t+T-1} F(k)\tilde{W}(k|t)\Delta t + \alpha \sum_{k=t}^{t+T-2}\sum_{j=1}^{N} D_j(k|t),$$

$$F(k) = \begin{cases} f^+(k) & \text{if } \tilde{W}(k|t) \geq 0 \\ f^-(k) & \text{if otherwise} \end{cases} \tag{1}$$

subject to

$\forall k \in \{t, \ldots, t+T-1\}$

$$\tilde{W}(k|t) = \tilde{W}^+(k|t) + \eta^{\mathrm{pv}}\tilde{W}^-(k|t) + \eta^{\mathrm{acdc}}\sum_{j=1}^{N} p_j^{\mathrm{v}}(k|t) + P^{\mathrm{standby}} \tag{2}$$

$$W_{\min} \leq \tilde{W}(k|t) \leq W_{\max} \tag{3}$$

$$\sum_{k=t}^{t+T-1} \tilde{W}(k|t)\Delta t \leq J_{\max} \tag{4}$$

$$\tilde{W}^+(k|t) + \eta^{\mathrm{acdc}}\sum_{j=1}^{N} p_j^{\mathrm{v}}(k|t) + P^{\mathrm{standby}} \geq 0 \tag{5}$$

$$p_j^{\mathrm{v}}(k|t)\tilde{\gamma}_j(k|t) = 0, \tag{6}$$

$$P_j^{\mathrm{v,dis}} \leq p_j^{\mathrm{v}}(k|t) \leq P_j^{\mathrm{v,char}} \tag{7}$$

$$B_j^{\mathrm{v,min}}(k|t) \leq b_j^{\mathrm{v}}(k|t) \leq B_j^{\mathrm{v,max}} \tag{8}$$

(Battery dynamics)

$$b_j^{\mathrm{v}}(k+1|t) = b_j^{\mathrm{v}}(k|t) + \{1-\tilde{\gamma}_j(k|t)\}Hp_j^{\mathrm{v}}(k|t)\Delta t - \tilde{\gamma}_j(k|t)\tilde{B}_j^{\mathrm{v,cons}}(k|t), \tag{9}$$

$$H = \begin{cases} \eta^{\mathrm{char}} & \text{if } p_j^{\mathrm{v}}(k|t) \geq 0 \\ \eta^{\mathrm{dis}} & \text{if otherwise} \end{cases}$$

$$D_j(k|t) \geq p_j^{\mathrm{v}}(k+1|t) - p_j^{\mathrm{v}}(k|t) \tag{10}$$

$$-D_j(k|t) \leq p_j^{\mathrm{v}}(k+1|t) - p_j^{\mathrm{v}}(k|t). \tag{11}$$

The objective function given by (1) is the summation of electricity costs, which is calculated by multiplying the predicted net power $\tilde{W}(k|t)$ defined in (2) by a cost coefficient $F(k)$. $F(k)$ is switched depending on whether the power is for purchase or sale, i.e., whether $\tilde{W}(k|t)$ is positive or negative. The HEMS obtains income from the sale of electric power when $\tilde{W}(k|t)$ is negative, but the HEMS pays for electricity when $\tilde{W}(k|t)$ is positive. Thus, the electricity cost is defined as a signed cost of $\tilde{W}(k|t)$. The second penalty term in (1) plays a role of reducing the frequent alternation of charging and discharging electric power to mitigate the damage on the in-vehicle battery lifetime. In (1), α is a weighting function, and $D_j(k|t)$ has constraints given by (10) and (11). The minimization of second penalty term with these constraints is equivalent to minimization of $|p_j^{\mathrm{v}}(k+1|t) - p_j^{\mathrm{v}}(k|t)|$.

Equation (3) provides the upper and lower bounds for $\tilde{W}(k|t)$, which is specified by the request from power grid, i.e., an electric power company. Equation (4) is the upper bound of consumed electric power for one day. These constraints prevent excessive home power consumption.

Equation (5) prevents the stored power in the in-vehicle batteries from backflowing to the power grid because present regulation in some country (for example, Japan) prohibits reverse power flow from batteries. Note that η^{acdc} and P^{standby} are constants that indicate the conversion efficiency and standby power consumption of the ac/dc and dc/dc converter units shown in Fig. 1, respectively.

Equation (6) is the constraint on the charge and discharge of the in-vehicle battery in accordance with the vehicle state. The battery can charge and discharge only when the vehicle is at home ($\tilde{\gamma}_j(k|t) = 0$). Conversely, the battery cannot charge and discharge at home when the vehicle is disconnected to the home ($\tilde{\gamma}_j(k|t) = 1$).

Equation (7) represents the constraint on the charge and discharge performances of the in-vehicle battery. Equation (8) is the constraint on the electric energy of in-vehicle battery, where $B_j^{\mathrm{v,min}}(k|t)$ indicates the minimum electric energy required at t.

Equation (9) represents the discrete dynamics of the electric energy of in-vehicle battery $b_j^{\mathrm{v}}(k|t)$. The efficiency of charge and discharge in (9) is specified by different parameters (η^{char} and η^{dis}). As the result, the battery dynamics is represented by a switched linear dynamics. The real efficiency in (9) may not be constant due to the change of the environment, the lifetime of the battery, and so on. Consideration of these nonlinear characteristics, however, results in complex nonlinear optimization, and is not preferable for real-time implementation. The effect of modeling error of battery dynamics is experimentally discussed in Section VI-A.

Note that most of the battery management unit often informs the remaining electric energy as the state of charge (SOC). The relationship between the remaining battery charge $b_j^{\mathrm{v}}(t)$ and $SOC_j(t)$ can be described by the following equation:

$$b_j^{\mathrm{v}}(t) = B_j^{\mathrm{v,max}} \times \frac{SOC_j(t)}{100}. \tag{12}$$

Thus, the $SOC_j(t)$ is defined as a percentage of the $b_j^{\mathrm{v}}(t)$ over $B_j^{\mathrm{v,max}}$. Since the $SOC_j(t)$ is not an accumulation of the power, $p_j^{\mathrm{v}}(t)$, (12) does not include the efficiency H in (9).

In this optimization problem, the objective function given by (1) and the constraint given by (9) have logical branching. By applying the technique used in a mixed logical dynamical system formulation [31] to this problem, the logical branching can be converted into inequalities by introducing binary variables. As the result, this optimization problem is classified as an MILP.

Detail of the transformation from logical branching in (1) to inequalities are explained in the following. The branching whether $\tilde{W}(k|t)$ is positive or not is represented by the binary variable $\delta_1(k) \in \{0, 1\}$ as follows:

$$\begin{cases} [\delta_1(k) = 1] \leftrightarrow [\tilde{W}(k|t) \geq 0] \\ [\delta_1(k) = 0] \leftrightarrow [\tilde{W}(k|t) < 0]. \end{cases} \tag{13}$$

Here, an upper bound M_1 and a lower bound m_1 were set to satisfy $m_1 \leq \tilde{W}(k|t) \leq M_1$. The logical formula given by (13) is equivalently expressed by the following inequalities:

$$\begin{cases} \tilde{W}(k|t) \geq m_1\{\delta_1(k) - 1\} \\ \tilde{W}(k|t) \leq (M_1 + \varepsilon_1)\delta_1(k) - \varepsilon_1 \end{cases} \tag{14}$$

where ε_1 is a small positive number. Using $\delta_1(k)$, the objective function given by (1) is rewritten as

$$Z = \sum_{k=t}^{t+T-1} [f^+(k)\tilde{W}(k|t)\delta_1(k) + f^-(k)\tilde{W}(k|t)\{1 - \delta_1(k)\}]\Delta t. \tag{15}$$

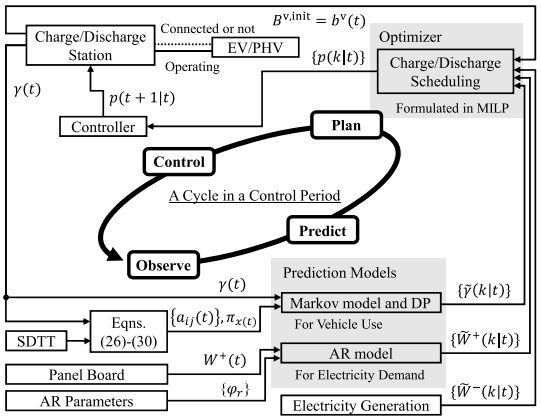

Fig. 2. Flow of information processing in the proposed HEMS.

Here, this objective function is nonlinear, because $\tilde{W}(k|t)$ and $\delta_1(k)$ are both decision variables in this optimization problem. To avoid the nonlinearity, the auxiliary variable $z_1(k)$ is introduced, which is defined as $z_1(k) = \tilde{W}(k|t)\delta_1(k)$. By using $z_1(k)$, (15) is rewritten as follows:

$$Z = \sum_{k=t}^{t+T-1} [\{f^+(k) - f^-(k)\}z_1(k) + f^-(k)\tilde{W}(k|t)]\Delta t. \tag{16}$$

In addition, $z_1(k) = \tilde{W}(k|t)\delta_1(k)$ is equivalently transformed to the following linear inequalities:

$$\begin{cases} z_1(k) \leq M_1\delta_1(k) \\ z_1(k) \geq m_1\delta_1(k) \\ z_1(k) \leq \tilde{W}(k|t) - m_1\{1 - \delta_1(k)\} \\ z_1(k) \geq \tilde{W}(k|t) - M_1\{1 - \delta_1(k)\}. \end{cases} \tag{17}$$

As the result, the original objective function (1), which has logical branching, is transformed to the one with binary variable and linear inequalities. The transformed optimization problem is solved as an MILP. Equation (9) is also transformed in the same way.

In order to improve the robustness of HEMS against the prediction and modeling errors, an MPC is exploited in this paper, which is based on the receding horizon prediction and optimization.

Fig. 2 illustrates a flow of information processing in the proposed control system. This consists of four functions, observation, prediction, planning, and control. The depicted cycle is executed in every Δt according to the receding horizon manner.

III. Prediction of Profile of Home Power Load

A. Data Set of Home Power Load

Electricity consumption of over 60 houses have been collected in the project of "Toyota City Low-Carbon Society Verification Promotion Council," for five years from 2010 to 2015 in Japan. In this paper, the data logging was executed every 1 min. For the proposed HEMS, first of all, the observed data of the home power load are preprocessed

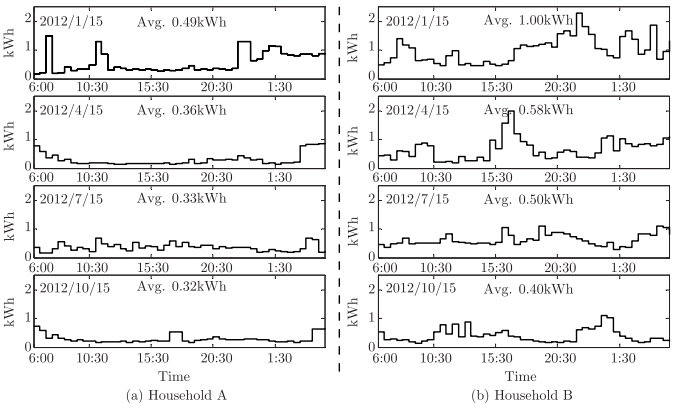

Fig. 3. Examples of home power load in four seasons. (a) Household A consists of two adults. (b) Household B consists of four adults and two children.

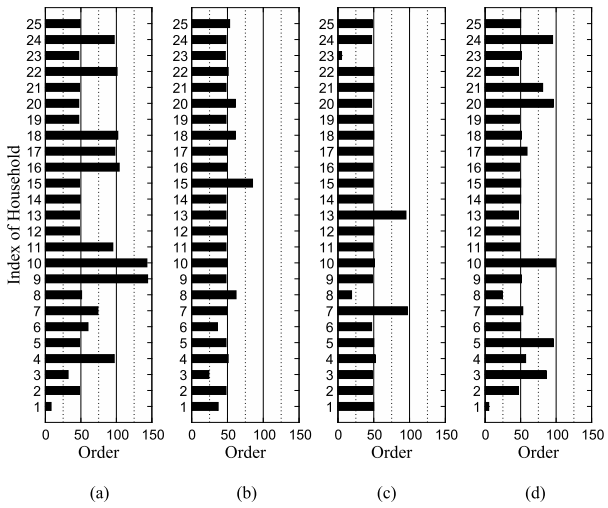

Fig. 4. Orders of the AR models using the AIC for 25 households and 4 seasons. (a) Winter. (b) Spring. (c) Summer. (d) Autumn.

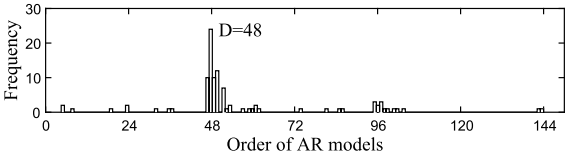

Fig. 5. Histogram of the order of the AR models.

to calculate the average power load every 30 min, that is the interval of one discrete time step Δt.

For example, several profiles of the home power load for 24 h are shown in Fig. 3. The profiles in the left side and the right side are obtained from households A and B, respectively. The household A consists of two adults, and the household B consists of four adults and two children. From top to bottom, the profiles show the selected one day from different seasons, winter, spring, summer, and autumn, respectively.

B. Prediction by Autoregressive Model

In this paper, an AR model is applied to prediction of future home power load. Suppose that the current time is t, and the past power load $W^+(t+1-r)$ $(r \in \{1, \ldots, R\})$ are already measured, the home power load $\tilde{W}^+(t+1|t)$ at the next time $t+1$ is estimated as follows:

$$\tilde{W}^+(t+1|t) = \sum_{r=1}^{R} \varphi_r W^+(t+1-r) + \epsilon_{t+1} \tag{18}$$

where $\varphi_r (r \in \{1, \ldots, R\})$ are coefficients called AR parameters, R is the order of the AR model, and ϵ_{t+1} is the output error at the time $t+1$. The parameters φ_r can be identified by minimizing the output errors using the least-mean-squares or Yule–Walker method in general.

1) Finding the Order of AR Model by AIC: In order to decide the order of the AR model properly, an Akaike information criterion (AIC) is used as an index [32]. The desirable model is the one which shows the minimum AIC value over the candidates of R for given data set. The AIC for AR model is defined as follows:

$$AIC \stackrel{\text{def}}{=} n(\ln(2\pi E) + 1) + 2(R+1) \tag{19}$$

where n is the number of data, and E is the average mean square of the AR model after identifying the AR parameters using the given data set. E is calculated as follows:

$$E = \frac{1}{n'} \sum_{\ell=1}^{n'} \epsilon_\ell^2 \tag{20}$$

where n' is the number of data used for identification.

As a preliminary experiment, the orders of AR models were identified by the AIC for 25 households in the range of $1 \leq R \leq 150 = R_{\max}$. The AR model of home power load prediction was built individually for each household and season, wherein January, April, July, and October were chosen as representative months. Each data set has 1440 data points of the power load in consecutive time steps Δt (=30[min]) for 30 days, which was observed in 2013. The desirable order of the AR model for each household and season, which shows the minimum AIC, is shown in Fig. 4. The vertical axis means the index number of the 25 households and the horizontal axis indicates the desirable order of the AR model defined by AIC. In addition, the histogram of the desirable order of AR models defined by AIC is shown in Fig. 5. These figures show that more than 90% of models have the order of $R = 48$ as the desirable one. In fact, we have found a strong autocorrelation between the home power loads $W^+(t)$ and $W^+(t-48)$. This comes from the periodic behavior of the home power load with a cycle of one day (48 steps). In general, the order of AR model should be defined individually for each household and season by referring the AIC. However, if there is no information on the home power load, the order of AR model R should be set to be 48.

2) Identified AR Parameters: As identification examples, AR parameters of the household no. 2 in the four seasons and the household no. 19 in the spring season are listed in Table I. To increase the understandability, this table displays only parameters which are greater than 0.05 or less than -0.05. As we can see, there are common characteristics in all AR models as follows: φ_1, φ_2, φ_{47}, and φ_{48} take relatively large values. This implies that the power load of $W^+(t)$, $W^+(t-1)$,

TABLE I
AR PARAMETERS FOR HOUSEHOLDS NO. 2 AND NO. 19

	Household no.2				Household no.19
φ_r	winter	spring	summer	autumn	spring
φ_1	0.714	0.507	0.615	0.771	0.732
φ_2	-0.090		-0.136	-0.161	
φ_3		0.077		0.105	-0.079
φ_4		-0.059	0.066		0.129
φ_5					-0.083
φ_6					0.060
φ_7			0.058		
φ_8				0.075	
φ_{12}			0.064		
φ_{13}		0.065			
φ_{16}			-0.056	0.066	
φ_{17}	0.056				0.072
φ_{20}					0.055
φ_{21}					-0.068
φ_{22}	0.076				
φ_{23}				-0.064	
φ_{24}		0.076		0.097	-0.055
φ_{25}	0.076		0.062	-0.073	
φ_{26}			-0.056		
φ_{27}		0.054			
φ_{28}				0.054	
φ_{30}	0.056				
φ_{32}					-0.058
φ_{33}			0.057		
φ_{36}			0.071		
φ_{39}	-0.053				
φ_{41}		-0.058			
φ_{44}	0.056				0.063
φ_{45}					-0.061
φ_{47}	0.095	0.068	0.107	0.098	0.055
φ_{48}	0.116	0.130	0.155		0.080

$W^+(t-47)$ and $W^+(t-46)$ play important roles for prediction. $W^+(t)$ is the current power load, $W^+(t-1)$ is the latest power load, i.e., 30 min before, $W^+(t-47)$ is the power load one day before from the time $t+1$ (target time of prediction), and $W^+(t-46)$ is the power load one day before from the next time $t+2$. Thus, the prediction of home power load basically uses the periodic characteristics of the home power load with the cycle of 24 h.

Despite the common characteristics in the structure of the AR model, the AR parameters take different values depending on household and season. This implies that the description performance of the AR model is not so powerful. Therefore, it is highly recommended to use different AR models according to the environmental condition. The use of multiple AR models will increase the prediction accuracy of the power load.

3) Cross Validation: The prediction error of the AR model is verified with k-fold cross validation. The data used to estimate the desirable order of AR model were divided into 30 subsets, i.e., each subset corresponds to the data of one day. The subsets of the first three days were not used for the cross validation. One subset was used for test and the remaining subsets were used for identification of the AR parameters. As the tests are carried out repeatedly for each subset in the k-fold cross validation, then the cross validation was executed as for 27 subsets from the 25 households and 4 seasons.

Fig. 6 shows the root mean squared errors (RMSEs) of the AR models as the result of cross validation. The horizontal axis represents the index number of the household.

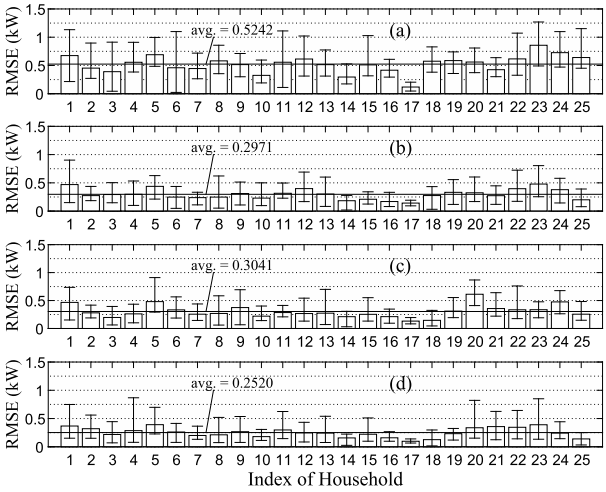

Fig. 6. RMSE in cross validation for the prediction of home power load. (a) Winter. (b) Spring. (c) Summer. (d) Autumn.

The average of RMSE for all of the tests is indicated by the height of bar together with the error range, which expresses the range between the maximum and minimum of the RMSEs. The results show that the RMSEs are less than 500 W in almost all cases except winter season. This is because the home power load in winter is higher than the one in other seasons. Although more complex prediction model may reduce the prediction errors, the average of the errors in the AR model is acceptable for the proposed HEMS.

4) Adaptation to the Proposed HEMS: In order to embed the AR model into the proposed HEMS, a slight modification must be made in (18). Since the receding horizon control needs to predict the home power load for T steps ahead ($T = 48$), the AR model needs to use the predicted values recursively instead of measured values. In this case, the following modified AR model must be used:

$$\tilde{W}^+(t+\tau|t) = \sum_{r_1=1}^{\tau-1} \varphi_{r_1} \tilde{W}^+(t+\tau-r_1|t) + \sum_{r_2=\tau}^{R} \varphi_{r_2} W^+(t+\tau-r_2). \quad (21)$$

Using the modified AR model (21), the predicted profile of the home power load becomes available for the proposed HEMS. Note that the trend of RMSE may increase as the time progress if we use (21) for prediction. Even in this case, however, the analyses shown in this section are effective.

IV. PREDICTION OF FUTURE VEHICLE STATE SEQUENCE

A. Statistics of Departure and Travel Time

For the prediction of future vehicle state $\gamma(t)$, the statistics of departure and travel time (SDTT) is supposed to be available at each household. The SDTT is described as a frequency distribution table, as shown in Table II. The frequency distribution table is generated by observing and collecting the departure time and arrival time of the vehicle every day. The column and the row express the departure and travel times, respectively. Note that the travel time is calculated

TABLE II
SDTT

		Departure time						
		6:00	6:30	7:00	7:30	⋯	5:00	5:30
		1	2	3	4	⋯	$T-1$	T
Travel time	0	91	86	72	50	⋯	95	92
	1	3	1	2	4	⋯	1	0
	2	2	1	1	6	⋯	0	1
	⋮	⋮	⋮	⋮	⋮	⋱	⋮	⋮
	$T-1$	1	3	1	2	⋯	1	2
	T	0	1	0	1	⋯	1	0

by subtracting the departure time from the corresponding arrival time. For example, the elements on the third row and the fourth column indicates six, it implies that there were six samples observed in the past that the vehicle left home at 7:30 and traveled for two steps (1 h) before returning home.

The number of columns is set to be T, which is the same as prediction length in the MPC. In addition, the data whose travel time exceeds T were excluded from the table. Therefore, the number of rows was set to be $T+1$. The travel time "0" in the first row implies that the vehicle was connected to the home, i.e., was available for HEMS.

B. Semi-Markov Model for Vehicle State Prediction

One of the most promising scenarios for the prediction of the future vehicle state is to formulate the problem so as to maximize the occurrence probability (score) of the predicted profile of the vehicle state. Since the number of possible vehicle state profile increases according to the increase of T, it is highly recommended to design the semi-Markov model, which represents the information included in the SDTT, and apply the search algorithm based on DP.

Here, let $X(t)$ be a random variable which represents the distribution of remaining travel time at t of the vehicle, i.e., the time until arriving at home. Also, let $x(t) \in \{0, 1, \ldots, T\}$ be the realization of $X(t)$ at time t. When the vehicle is connected to the home, $x(t)$ takes a value of zero. If the vehicle leaves the home at t, the state $x(t) = 0$ transits to the state $x(t+1)$ which takes some value between 1 to T. This transition is defined stochastically from the SDTT. Then, $x(t+1)$ decreases monotonically step by step, i.e., $x(t+i) = x(t+i-1) - 1$. This state definition implies that one of the vehicle states $\gamma(t) = 1$ is expanded to multiple states $x(t) = 1 \sim T$. The behavior of $x(t)$ is expressed by a left-to-right semi-Markov model shown in Fig. 7.

It is necessary to consider the states up to $t + 2T$, because there is a case that the vehicle leaves home at $t + T$ and returns to home after T-steps travel at most. However, since the departure time to be predicted is restricted in the range of T steps (one day) from the present time, the states after $t + T$ have no transition from $x(\tau) = 0$ $(\tau \geq t + T)$ to the other states except for $x(\tau + 1) = 0$.

The next step is to design the transition probability and initial state probability in the semi-Markov model. The transition probability from the state j to i at time t is described as

$$a_{ij}(t) = P(X(t+1) = i \,|\, X(t) = j). \tag{22}$$

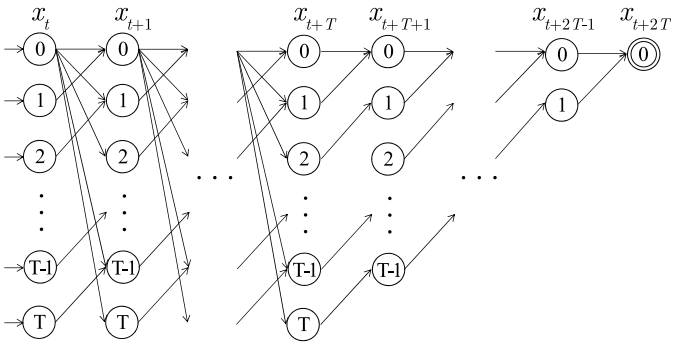

Fig. 7. Left-to-right semi-Markov model of a remaining travel time.

Note that the transition probability is a time varying parameter. This transition probability can be defined from the SDTT as follows.

Let c_{nm} be an element of the SDTT at nth row and mth column (see Table II). At first, the transition probability from state $x(t) = 0$, i.e., $a_{i0}(t)$ is calculated as follows:

$$a_{i0}(t) = \frac{c_{\tau i}}{\sum_{i=0}^{T} c_{\tau i}}$$
$$\tau = t \bmod T \tag{23}$$

where τ is the time index in Table II. Once the vehicle state takes a nonzero value (vehicle leaves home), the remaining travel time to the home decreases monotonically step by step. Therefore, other state transition probabilities $a_{ij}(t)$ for $j > 0$ are defined as

$$a_{ij}(t) = \begin{cases} 1 & i = j - 1 \\ 0 & i \neq j - 1. \end{cases} \tag{24}$$

Since the vehicle state prediction is executed in receding horizon manner, i.e., the vehicle state prediction is updated at every control cycle based on the new observation, the initial state probability of the semi-Markov model must be updated at every step. Let π_{x_t} be the initial state probability of the state $x_t \in \{0, 1, \ldots, T\}$ at t. In the case that the vehicle is connected to the home at t, i.e., $\gamma(t) = 0$, the remaining travel time x_t must be zero. Therefore

$$\pi_{x(t)=0} = 1$$
$$\pi_{x(t)\neq 0} = 0. \tag{25}$$

On the other hand, in the case that the vehicle is not connected to the home (used for transportation), i.e., $\gamma(t) = 1$, the initial state probability at t can be calculated based on the latest departure time s_0 $(s_0 < t)$. This is obvious because the current initial state probability can be calculated using the information on the latest departure time of the vehicle. Note that the actual departure of the vehicle occurs between $s_0 - 1$ and s_0. As the result, in the case that the vehicle is not connected to the home, i.e., $\gamma(t) = 1$, the initial state probability at t and $\pi_{x(t)}$

is calculated as

$$\begin{aligned}\pi_{x(t)} &= P(X(s_0-1)=0 \\ &X(s_0)\neq 0, \quad X(s_0+1)\neq 0,\ldots,X(t)\neq 0) \\ &= \begin{cases} \dfrac{a_{(i+t-s_0)0}(t)}{\sum_{j=t-s_0}^{T} a_{j0}(t)}, & 0\le i\le T-t+s_0 \\ 0 & T-t+s_0<i\le T. \end{cases}\end{aligned} \tag{26}$$

Finally, note that the occurrence probability of the path from $x(t+T)=i$ to $x(t+2T)=0$ (accepted stated) is equal to one because each path from the state $x(t+T)=i$ to the accepted state $x(t+2T)=0$ is deterministic.

C. Finding of Most Likely State Sequence by Dynamic Programming

The most likely future state (remaining travel time) sequence can be found by applying DP thanks to Markov characteristics described in the last section. The prediction problem is now formulated as follows.

Prediction of the Remaining Travel Time:

$$\begin{aligned}&\textbf{Given}: s_0, \gamma(t), \{a_{ij}(t)\}_{i,j\in\{1,\ldots,T\}} \\ &\textbf{find}: x(t),\ldots,x(t+T),\ldots,x(t+2T) \\ &\textbf{which maximize}: \\ &J = P(X(t)=x(t), X(t+1)=x(t+1)\ldots, \\ &X(t+T)=x(t+T),\ldots,X(t+2T)=x(t+2T)).\end{aligned} \tag{27}$$

This prediction is executed at every control cycle, i.e., every 30[min]. The cost function (27) can be rewritten by using parameters in semi-Markov model. Then, the best score J^* is defined as

$$\begin{aligned}J^* = \max_{x(t),\ldots,x(t+T)} &[\pi_{x(t)} a_{x(t+1)x(t)}(t) a_{x(t+2)x(t+1)}(t+1)\cdots \\ &a_{x(t+T)x(t+T-1)}(t+T-1)].\end{aligned} \tag{28}$$

This maximization can be decomposed as follows:

$$\begin{aligned}J^* = &\max_{x(t+T)} a_{x(t+T)x(t+T-1)}(t+T-1) \\ &* \left\{ \max_{x(t),\ldots,x(t+T-1)} [\pi_{x(t)} a_{x(t+1)x(t)}(t) a_{x(t+2)x(t+1)}(t+1) \right. \\ &\left. * \cdots a_{x(t+T-1)x(t+T-2)}(t+T-2)] \right\}.\end{aligned} \tag{29}$$

Here, the following variables are introduced:

$$\begin{aligned}&\delta(\tau, x(\tau)) \\ &= \begin{cases} \pi_{x(t)} & \tau = t \\ \max\limits_{x(\tau-1)} [\delta(\tau-1, x(\tau-1)) a_{x(\tau)x(\tau-1)}(\tau-1)] & \tau \ge t+1 \end{cases}\end{aligned} \tag{30}$$

and for $\tau \ge t+1$

$$\psi(\tau, x(\tau)) = \arg\max_{x(\tau-1)} [\delta(\tau-1, x(\tau-1)) a_{x(\tau)x(\tau-1)}(\tau-1)]. \tag{31}$$

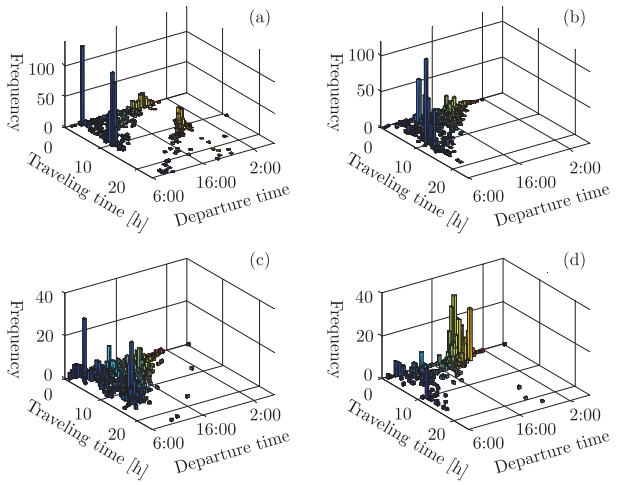

Fig. 8. Examples of SDTT corrected from households wherein the vehicle is mainly used for (a) and (b) commutation to office and (c) and (d) shopping and pickup. Note that the scale of vertical axis, frequency, is different graph by graph.

By substituting (30), (29) is expressed as

$$\begin{aligned}J^* = \max_{x(t+T)} &[a_{x(t+T)x(t+T-1)}(t+T-1) \\ &* \delta(t+T-1, x(t+T-1))].\end{aligned} \tag{32}$$

This implies that J^* can be calculated recursively from $\tau = t$ to $\tau = t+T$. The final state $x^*(t+T)$ is found in the recursive calculation of J^* as follows:

$$\begin{aligned}x^*(t+T) = \arg\max_{x_{t+T}} &[a_{x(t+T)x(t+T-1)}(t+T-1) \\ &\delta(t+T-1, x(t+T-1))].\end{aligned} \tag{33}$$

The states after $t+T$ are generated by

$$x^*(\tau+1) = \begin{cases} x^*(\tau)-1 & x^*(\tau)\neq 0 \\ 0 & x^*(\tau)=0 \end{cases} \tag{34}$$

for $\tau \ge t+T$. The most likely states before $t+T$ can be found by the following backward calculation:

$$x^*(\tau) = \psi(\tau+1, x^*(\tau+1)) \quad t\le\tau\le t+T-1. \tag{35}$$

As the result, the most likely state sequence $x^*(t+i)$ $(i=0\sim 2T)$ can be obtained. Once $x^*(t+i)$ $(i=0\sim 2T)$ is obtained, it can be transformed to the most likely vehicle state sequence $\gamma^*(t+i)$ $(i=0\sim 2T)$ by using

$$\gamma^*(t+i) = \begin{cases} 0 & \text{if } x^*(t+i)=0 \\ 1 & \text{if } x^*(t+i)=1\sim T. \end{cases} \tag{36}$$

D. Evaluation of Vehicle State Prediction

Fig. 8 shows the examples of SDTT corrected from examinees who use a vehicle for her/his daily life. Note that the frequency data whose traveling time is zero are omitted for visibility. The data were corrected for 27 months from 30 examinees by equipping GPS loggers on their vehicles. The examinees are categorized into two groups based on their purpose to use the vehicle, for commuting to office or for other purposes like shopping and picking up a child.

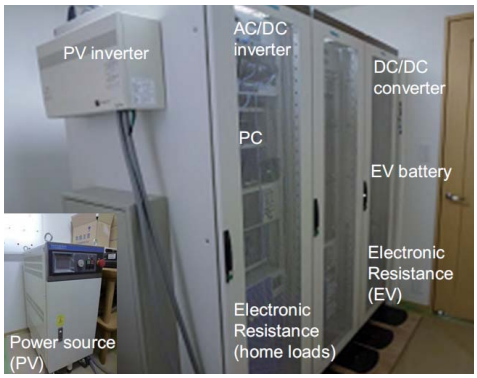

Fig. 9. HEMS experimental testbed used to test the proposed control scheme, each component is scaled down by a factor of 3.

TABLE III
SPECIFICATIONS OF THE HEMS EXPERIMENTAL TESTBED

Equipment	Simulator	Capacity
PV	DC power sources	5kW
PV inverter	–	4.5kW
Home load	Electric resistance	2 kW
EV	Electric resistance	3kW
EV battery	–	3 kWh
DC/DC converter	–	2.5 kW
AC/DC inverter	–	2.5 kW

The SDTTs [Fig. 8(a) and (b)] are corrected from two examinees who use the vehicle mainly for commute to office, and [Fig. 8(c) and (d)] are from two examinees who use the vehicle for other purposes. Generally speaking, one who uses the vehicle with regularity has peaks on her/his SDTT, and is easy to predict her/his use of vehicle.

The proposed prediction method was evaluated based on accuracy rate. The accuracy rate is calculated as agreement rate of PDTTs between prediction and observation. In this calculation, the data of 24 months was used for learning the parameters in the semi-Markov model and the remaining 3 month data was used for evaluation. The mean value of accuracy rate of 30 examinees was 0.77 and the standard deviation was 0.22. The accuracy rate of 0.77 which is much larger than 0.5 implies the validity of proposed prediction method. In addition, the update mechanism of the prediction model based on the automatic update of the statistical data improves the accuracy rate of the prediction.

V. VERIFICATION BY HEMS EXPERIMENTAL TESTBED

A. Experimental Setup

The proposed control scheme is implemented on the HEMS experimental testbed shown in Fig. 9. The specifications of the testbed are listed in Table III. This testbed consists of several physical simulators to represent the PV generation, home load, and in-vehicle batteries. The electrical characteristics of all components are scaled down by a factor of three from those of actual components. In this testbed, a single vehicle (EV) is considered, which can only be charged or discharged when it is connected to the home. Departure and arrival of the vehicle are realized by disconnecting and reconnecting the physical simulator of the in-vehicle battery. Energy consumption of the EV while driving is simulated by extracting power from the in-vehicle battery by using an electronic resistance. The control architecture for this testbed has two-layered structure [8]. The first layer, where the algorithm in Section II is implemented, decides the optimal charge/discharge plan for the in-vehicle battery to reduce the daily electricity cost. The second layer consists of a dc/dc converter and an ac/dc inverter. This layer adopts the voltage-based droop control principle [33], [34], and can maintain the instantaneous supply–demand balance even if there is a mismatch between the plan and the actual situation caused by the prediction and modeling errors.

TABLE IV
PARAMETER SETTING

Parameter	Unit	Value	
$f^+(t)$	Yen/kWh	9 21 31 21	23:00–7:00 7:00–9:00 9:00–17:00 17:00–23:00
$f^-(t)$	Yen/kWh	48	
$W_{\max}$	W	2500	
$J_{\max}$	Wh	50000	
$P_j^{\mathrm{v,char}}$	W	2000	
$P_j^{\mathrm{v,dis}}$	W	2000	
$B_j^{\mathrm{v,max}}$	Wh	3000	
$B_j^{\mathrm{v,init}}$	Wh	3000	
η^{char}	–	0.99	
η^{dis}	–	1.01	
η^{pv}	–	0.9	
η^{acdc}	–	1.03	
P^{standby}	W	120	

The parameters defined in the formulation given in Section II are listed in Table IV. According to the rate plan provided by a local power company [35], the purchase price $f^+(t)$ of power from the power grid varies with time, as shown in Table IV. The sale price $f^-(t)$ of power to the power grid is fixed at 48 Yen/kWh. As mentioned in Section II, the MPC cycle (Δt) was set to be 30 min, and continuously operated.

B. Data Used for Prediction

Fig. 10 depicts the actual (thick line) and predicted (thin lines) home load by using AR model with 48th order at each control step. The actual home load is the one observed in a household in the "Toyota city project" on a weekday in winter. The receding horizon prediction results predicted at 4:00, 5:00, 6:00, 7:00, 8:00, 12:00, 16:00, and 20:00 are depicted. As a whole, although errors exist between the prediction and actual value especially when the home load is high, the 48th order AR model can successfully predict the home load by receding horizon manner. In order to improve the prediction performance, the parameters of AR model must be adaptively switched according to change of day of the week, weather, season, and so on.

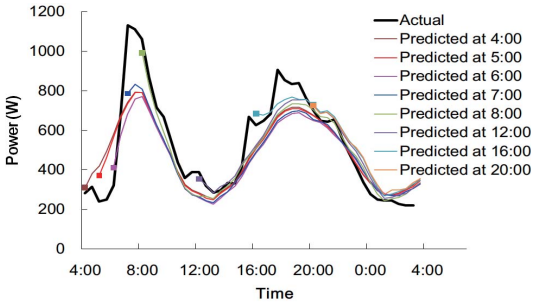

Fig. 10. Predicted home power load at each control step (thin lines) and actual home power load (thick line).

As for the prediction of vehicle state, the data where the vehicle is mainly used for commute to office (see Section IV) were used as the SDTT.

VI. Results and Discussion

A. Effectiveness of MPC

The benefits of using MPC are: 1) its robustness caused by a feedback mechanism underlying the MPC and 2) consideration of many important constraints. In this section, some experimental results are shown and discussed mainly focusing on the robustness. Note that the prediction error of the home load shown in Fig. 10 is considered in all experiments, which is caused by the limitation of the accuracy of the AR model. A commercial software CPLEX was used to solve MILP in all experiments.

1) Case of Existence of Prediction Error in Battery SOC: The SOC of in-vehicle battery is an important variable for optimization because charge/discharge of in-vehicle battery is highly dependent on the SOC of the battery. Therefore, it is critical to precisely estimate the SOC on the basis of the battery model. Herein, a simple switched linear model has been adopted in Section II [see (9)] for estimation of the SOC in order to reduce the computational burden. This model tends to achieve low precision for SOC estimation, because most batteries demonstrate nonlinear charge/discharge characteristics depending on the environmental conditions. Figs. 11 and 12 show the scheduled and actual results of charge/discharge of the in-vehicle battery and SOC based on the single prediction and optimization executed at 4:00 in the cases of $\alpha = 0$ and $\alpha = 0.01$ [see (1)], respectively. Figs. 13 and 14 show the scheduled and actual results with MPC, i.e., the prediction and optimization are updated every 30[min] in the cases of $\alpha = 0$ and $\alpha = 0.01$, respectively. Both results are obtained under the perfectly predicted scenario as for the vehicle state. The EV is away from home during the hours 11:00–17:00. In Fig. 11(a), the charge/discharge profile of the in-vehicle battery for all 48 time steps was determined at the first time step, and executed. We can see that the errors between the estimated SOC and actual SOC are increasing with time because of modeling error of battery dynamics. During the hours 18:00–0:00, the battery's actual capacity for useful discharge remained unutilized, because the estimated SOC has dropped to the lower limit [Fig. 11(b)].

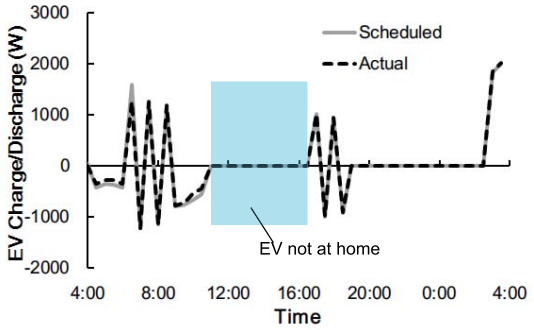

(a)

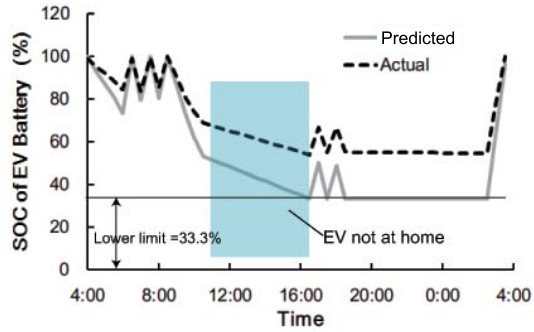

(b)

Fig. 11. Results based on single prediction and optimization executed at 4:00 in the case of $\alpha = 0$ and prediction error in battery SOC. (a) Charge/discharge profile of in-vehicle battery (charge: positive and discharge: negative). (b) Profile of battery SOC (actual and prediction at 4:00).

In the results with MPC [Fig. 13(a) and (b)], the estimated SOC is updated by measurements at each control step. According to the receding horizon prediction and optimization based on the updated information on the battery SOC, the in-vehicle battery becomes available for discharge during the hours 18:00–0:00 [Fig. 13(a)]. These results verify the robustness of MPC against the modeling error of battery dynamics.

Note that frequent alternation of charging and discharging appears in Figs. 11 and 13. This is because the charge and discharge efficiencies of the in-vehicle battery (see Table IV) were set to be high values, which had less impact on the energy loss. On the other hand, we can see that frequent alternation of charging and discharging can be effectively reduced in Figs. 12 and 14 in comparison with Figs. 11 and 13 by considering the penalty term in (1). It is also possible to reduce the frequent alternation by raising η^{dis} or lowering η^{char}.

2) Case of Existence of Prediction Error in Vehicle State: The availability of the in-vehicle battery directly affects on the performance of the HEMS for electricity cost reduction. Poorly predicted vehicle state sequence can lead to degradation of cost reduction performance. With MPC, the prediction of vehicle state sequence was updated by the sensing information (whether the EV is connected to home). Fig. 15(a) and (b) shows the results of prediction and scheduling based on the single prediction and optimization at 4:00 ($\alpha = 0$). Fig. 16(a) and (b) shows the results of prediction and scheduling with MPC, i.e., the prediction and the optimization

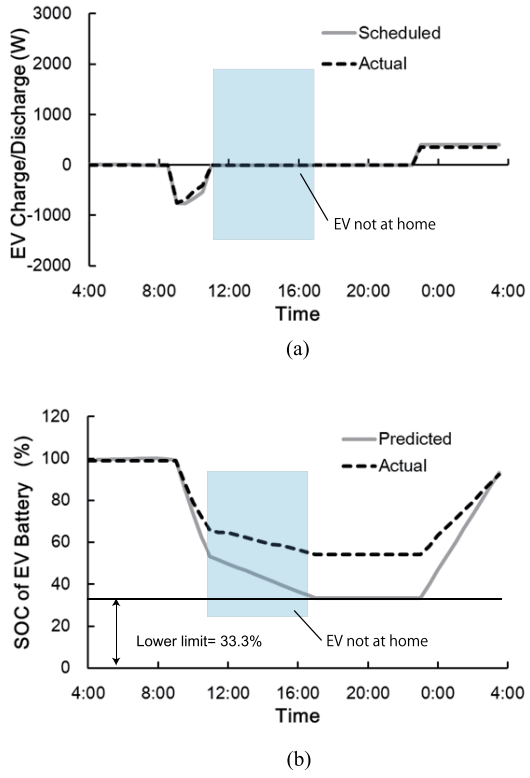

Fig. 12. Results based on single prediction and optimization executed at 4:00 in the case of $\alpha = 0.01$ and prediction error in battery SOC. (a) Charge/discharge profile of in-vehicle battery (charge: positive and discharge: negative). (b) Profile of battery SOC (actual and prediction at 4:00).

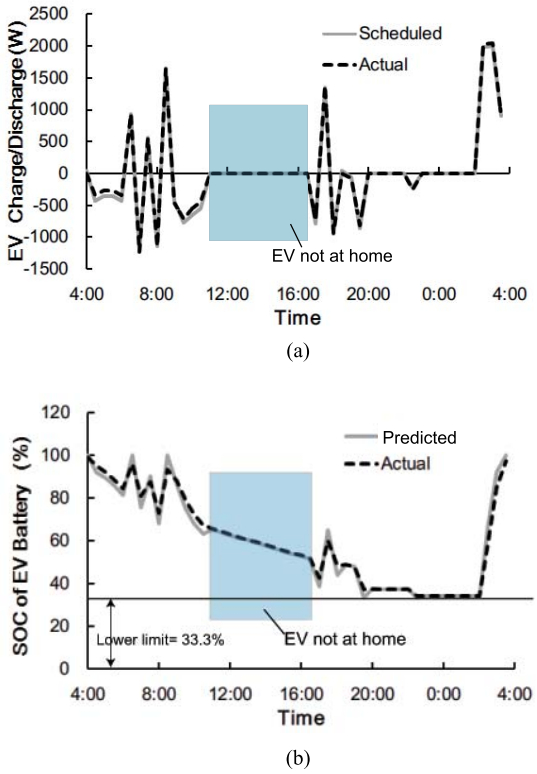

Fig. 13. Results with MPC (receding horizon prediction and optimization) in the case of $\alpha = 0$ and prediction error in battery SOC. (a) Charge/discharge profile of in-vehicle battery (charge: positive and discharge: negative). (b) Profile of battery SOC.

TABLE V
DAILY ELECTRICITY COST (YEN) FOR CASES 1 TO 3

α	case 1	case 2	case 3
$\alpha = 0$	92.7	90.1	39.5
$\alpha = 0.01$	92.7	92.6	49.1

are updated every 30[min] ($\alpha = 0$). In Fig. 15(b), the charge/discharge profile of the in-vehicle battery is scheduled on the basis of the predicted vehicle state sequence at 4:00, as shown in Fig. 15(a). According to the prediction, the EV would be away from home during the hours 17:00–19:00, and the in-vehicle battery was scheduled not to charge/discharge during this period even though the EV was actually at home and available for power storage. In the results with MPC shown in Fig. 16(b), the prediction of vehicle state was updated at 11:30 as shown in Fig. 16(a) by sensing the information on availability of the EV. According to the rescheduled plan, which is updated based on the updated prediction of vehicle state, the in-vehicle battery became available for charge or discharge during the hours 17:00–19:00. These results verify the robustness of MPC against the prediction error.

B. Economic Benefits of the Proposed HEMS

In order to evaluate the economic benefits of applying the proposed HEMS, the daily electricity cost is considered for evaluation. Herein, the electricity cost for one day is defined as the cost of purchasing power from the power grid minus the benefits of selling power to the power grid. For comparison, the daily electricity costs under different conditions represented by three cases are investigated. In case 1, the EV was used strictly as a vehicle and provided no benefit for energy management. In case 2, the EV served a dual purpose of transportation and storage for the HEMS. The EV was used during the hours 8:00–19:00 (i.e., EV was connected to home for 13 h). Case 3 is similar to case 2, wherein the EV was used for driving during the hours 11:00–17:00 (i.e., EV was connected to home 18 h). The availability of the in-vehicle battery in case 3 is higher than that in case 2. For simplicity, it is assumed that the actual home load and the PV output were equivalent for all three cases. The comparison of results of the daily electricity cost for three cases is shown in Table V. In this comparison, the price profiles $f^+(t)$ and $f^-(t)$ shown in Table IV were used.

In the case of $\alpha = 0$, the daily electricity costs for cases 1–3 were 92.7, 90.1, and 39.5 Yens, respectively. Compared with case 1, the daily electricity cost was reduced by 3% and 57% for cases 2 and 3, respectively. In cases 1 and 2, the amounts of PV power sold to the grid are practically equivalent because of the absence of a storage battery during the period of PV output. However, the purchase cost in case 2 is lower than that in case 1, because the power purchased from the power grid was shifted from the high-priced period to the low-priced period by the HEMS using the in-vehicle battery as power storage in case 2. Compared with case 2, the higher availability

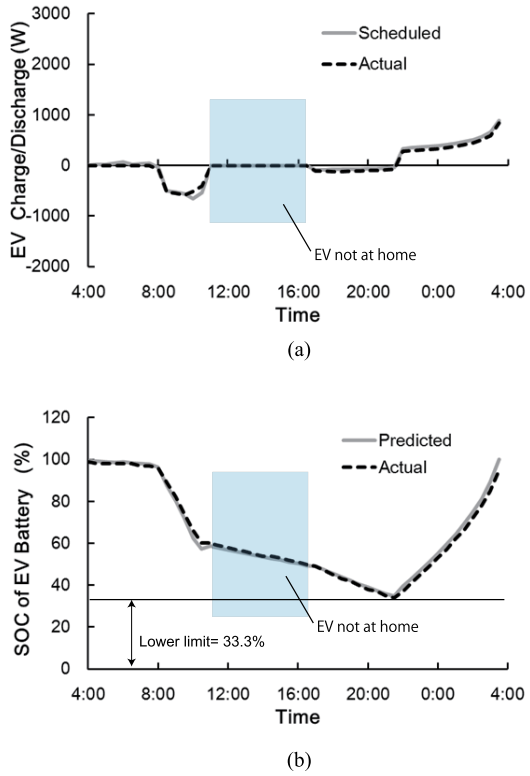

Fig. 14. Results with MPC (receding horizon prediction and optimization) in the case of $\alpha = 0.01$ and prediction error in battery SOC. (a) Charge/discharge profile of in-vehicle battery (charge: positive and discharge: negative). (b) Profile of battery SOC.

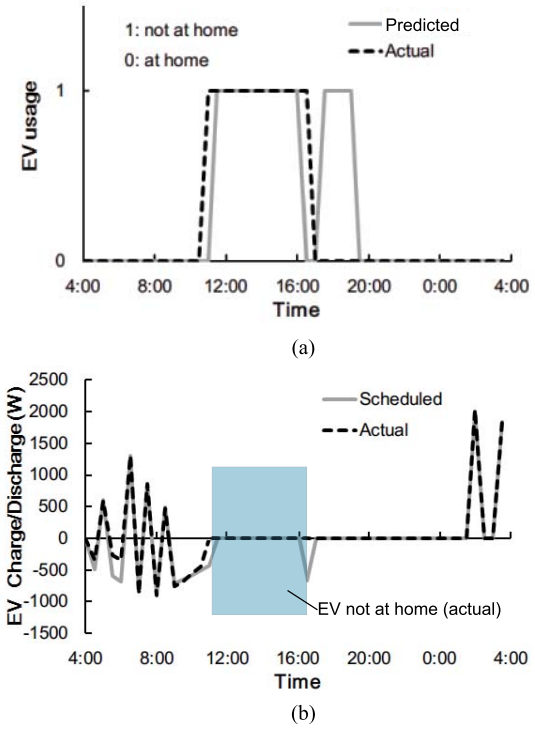

Fig. 15. Results based on single prediction and optimization executed at 4:00 in the case of $\alpha = 0$ and prediction error in vehicle state. (a) Profile of vehicle state predicted at 4:00. (b) Charge/discharge profile of in-vehicle battery (charge: positive and discharge: negative).

of the in-vehicle battery in case 3 provided greater opportunity for battery discharge to achieve higher sale benefit.

In the case of $\alpha = 0.01$, the daily electricity costs for cases 1–3 were 92.7, 92.6, and 49.1 Yens, respectively. A similar trend as the results of $\alpha = 0$ can also be found. However, the daily electricity costs of cases 2 and 3 in the case of $\alpha = 0.01$ are higher than those in the case of $\alpha = 0$ due to reducing the degree of freedom in charging and discharging of the in-vehicle battery.

C. Discussion

1) One of the advantages of the MPC is to take into consideration the several constraints, which is generally not easy in the conventional feedback control schemes. On the other hand, it is very important to design the constraints carefully so as to find a feasible solution at any time. For example, the minimum SOC $B_j^{v,\min}$ must be specified under the consideration of emergent use of the vehicle. In general, $B_j^{v,\min}$ for PHV can be set to be smaller than that for EV.
2) If there exists a huge amount of prediction error in the power load and/or vehicle state, the MPC may not work well. This is also the case that some emergency events and/or urgent vehicle use by the user happen. The proposed scheme, however, is likely to be able to keep the overall system stable thanks to the two-layer control structure (i.e., upper level: MPC and lower level: droop control, see Section V-A), because the lower level controller is designed to maintain the instantaneous supply–demand balance at any time. This is also effective for the case that unreasonable constraints are specified.
3) The electricity price profile was supposed to be given *a priori*, and the selling and buying prices are different. This is common in Japan and some other countries, which try to accelerate the penetration of renewable energy. The fusion of the proposed HEMS with real-time pricing systems like day ahead or hour ahead power market will lead to a development of HEMS aggregator, which takes a balance of requirements of both each household and grid.
4) Battery performance is strongly dependent on aging and temperature. Both factors can be taken into account in the proposed control system framework. The aging of the in-vehicle battery can be modeled by adjusting $B_j^{v,\max}$. If the capacity of in-vehicle battery is reduced due to aging, we should gradually decrease $B_j^{v,\max}$ to express the effect of aging. Note that the rate of decreasing $B_j^{v,\max}$ can be much slower than the control rate of HEMS. As for temperature, the performance variation caused by temperature can also be modeled by adjusting $P_j^{v,\mathrm{char}}$ and $P_j^{v,\mathrm{dis}}$. For example, if the ambient temperature around the battery is high, we should decrease the magnitudes of $P_j^{v,\mathrm{char}}$ and $P_j^{v,\mathrm{dis}}$ to mitigate the damage on battery health.
5) In this paper, only the best scored vehicle state sequence was exploited for the MPC. However, in our framework,

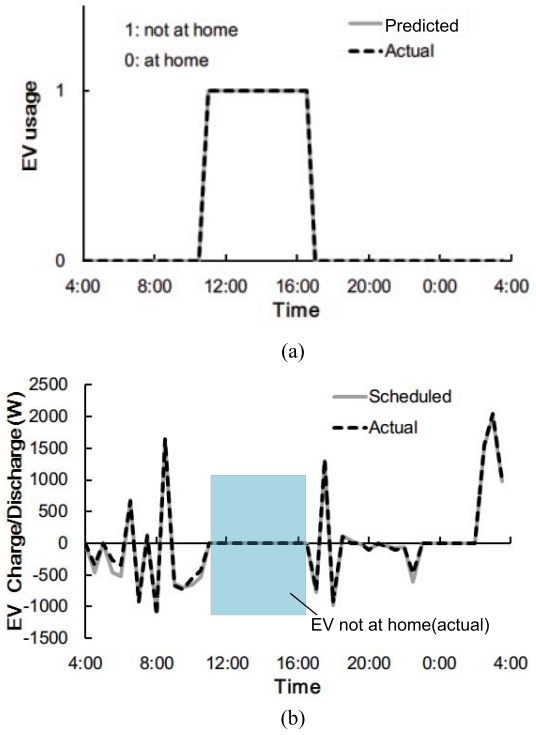

Fig. 16. Results with MPC (receding horizon prediction and optimization) in the case of $\alpha = 0$ and prediction error in vehicle state. (a) Profile of vehicle state updated at 11:30. (b) Charge/discharge profile of in-vehicle battery (charge: positive and discharge: negative).

other high-scored sequences such as the second and/or third best scored vehicle state sequences are also available for the MPC. In this case, the MPC may have a possibility to find better charging profiles than the case of considering only the best scored one. This deserves to be considered particularly if there is no big difference in the occurrence probability among the high-scored sequences.

VII. Conclusion

This paper has presented HEMS which integrates a prediction of future vehicle state and home load, optimization of the charge/discharge profile of the in-vehicle batteries, and real-time execution by using MPC framework. One of our main concerns was the development of prediction scheme of future vehicle state sequence, which can be naturally embedded in the MPC control framework. This was achieved by using DP over semi-Markov model which is designed based on statistical data of daily vehicle use. In order to minimize the daily home electricity costs, the proposed HEMS schedules the charge and discharge of the vehicle batteries in receding horizon manner. From the implementation of the proposed scheme on the HEMS experimental testbed, the following issues have been verified: 1) integration as the MPC, i.e., integration of prediction, optimization, and execution of charge/discharge of EV batteries under realistic constraints has been successfully made and executed in real time; 2) thanks to the receding horizon scheme, the proposed HEMS has robustness against the modeling and prediction error, such as battery dynamics, home load, and vehicle state; and 3) the proposed HEMS has economic potential benefits. The improvement of prediction scheme and the fusion of the proposed HEMS with real-time pricing systems will be our future works.

References

[1] S. M. Amin and B. F. Wollenberg, "Toward a smart grid: Power delivery for the 21st century," *IEEE Power Energy Mag.*, vol. 3, no. 5, pp. 34–41, Sep./Oct. 2005.

[2] T. Hahn, Z. Tan, and W. Ko, "Design of time-varying rate considering CO_2 emission," *IEEE Trans. Smart Grid*, vol. 4, no. 1, pp. 383–389, Mar. 2014.

[3] Z. Chen, L. Wu, and Y. Fu, "Real-time price-based demand response management for residential appliances via stochastic optimization and robust optimization," *IEEE Trans. Smart Grid*, vol. 3, no. 4, pp. 1822–1831, Dec. 2012.

[4] X. Liang, X. Li, R. Lu, X. Lin, and X. Shen, "UDP: Usage-based dynamic pricing with privacy preservation for smart grid," *IEEE Trans. Smart Grid*, vol. 4, no. 1, pp. 141–150, Mar. 2014.

[5] T. T. Kim and H. V. Poor, "Scheduling power consumption with price uncertainty," *IEEE Trans. Smart Grid*, vol. 2, no. 3, pp. 519–527, Sep. 2011.

[6] C. Chen, J. Wang, Y. Heo, and S. Kishore, "MPC-based appliance scheduling for residential building energy management controller," *IEEE Trans. Smart Grid*, vol. 4, no. 3, pp. 1401–1410, Sep. 2013.

[7] W.-Y. Chiu, H. Sun, and H. V. Poor, "Demand-side energy storage system management in smart grid," in *Proc. IEEE SmartGridComm*, Nov. 2012, pp. 73–78.

[8] A. Ito and T. Shiraki, "Optimal energy storage management in DC power networks," in *Proc. IEEE SmartGridComm*, Oct. 2013, pp. 630–635.

[9] W. Kempton and J. Tomić, "Vehicle-to-grid power fundamentals: Calculating capacity and net revenue," *J. Power Sour.*, vol. 144, no. 1, pp. 268–279, 2005.

[10] K. C. Divya and J. Østergaard, "Battery energy storage technology for power systems—An overview," *Electr. Power Syst. Res.*, vol. 79, no. 4, pp. 511–520, 2009.

[11] C. Liu, K. T. Chau, D. Wu, and S. Gao, "Opportunities and challenges of vehicle-to-home, vehicle-to-vehicle, and vehicle-to-grid technologies," *Proc. IEEE*, vol. 101, no. 11, pp. 2409–2427, Nov. 2013.

[12] Y. Ota, H. Taniguchi, T. Nakajima, K. M. Liyanage, J. Baba, and A. Yokoyama, "Autonomous distributed V2G (vehicle-to-grid) satisfying scheduled charging," *IEEE Trans. Smart Grid*, vol. 3, no. 1, pp. 559–564, Mar. 2012.

[13] S. Chen and L. Tong, "iEMS for large scale charging of electric vehicles: Architecture and optimal online scheduling," in *Proc. SmartGridComm*, Nov. 2012, pp. 629–634.

[14] F. Berthold, A. Ravey, B. Blunier, D. Bouquain, S. Williamson, and A. Miraoui, "Design and development of a smart control strategy for plug-in hybrid vehicles including vehicle-to-home functionality," *IEEE Trans. Transport. Electrific.*, vol. 1, no. 2, pp. 168–177, Aug. 2015.

[15] L. Jian, H. Xue, G. Xu, X. Zhu, D. Zhao, and Z. Y. Shao, "Regulated charging of plug-in hybrid electric vehicles for minimizing load variance in household smart microgrid," *IEEE Trans. Ind. Electron.*, vol. 60, no. 8, pp. 3218–3226, Aug. 2013.

[16] O. Erdinc, N. G. Paterakis, T. D. P. Mendes, A. G. Bakirtzis, and J. P. S. Catalão, "Smart household operation considering bi-directional EV and ESS utilization by real-time pricing-based DR," *IEEE Trans. Smart Grid*, vol. 6, no. 3, pp. 1281–1291, May 2015.

[17] M. Caramanis, E. Ntakou, W. W. Hogan, A. Chakrabortty, and J. Schoene, "Co-optimization of power and reserves in dynamic T&D power markets with nondispatchable renewable generation and distributed energy resources," *Proc. IEEE*, vol. 104, no. 4, pp. 807–836, Apr. 2016.

[18] D. T. Nguyen and L. B. Le, "Joint optimization of electric vehicle and home energy scheduling considering user comfort preference," *IEEE Trans. Smart Grid*, vol. 5, no. 1, pp. 188–199, Jan. 2014.

[19] S. Shahidinejad, E. Bibeau, and S. Filizadeh, "Statistical development of a duty cycle for plug-in vehicles in a North American Urban setting using fleet information," *IEEE Trans. Veh. Technol.*, vol. 59, no. 8, pp. 3710–3719, Oct. 2010.

[20] A. Ashtari, E. Bibeau, S. Shahidinejad, and T. Molinski, "PEV charging profile prediction and analysis based on vehicle usage data," *IEEE Trans. Smart Grid*, vol. 3, no. 1, pp. 341–350, Mar. 2012.

[21] C.-H. Wu, J.-M. Ho, and D. T. Lee, "Travel-time prediction with support vector regression," *IEEE Trans. Intell. Transp. Syst.*, vol. 5, no. 4, pp. 276–281, Dec. 2004.
[22] M. Chen and S. Chien, "Dynamic freeway travel-time prediction with probe vehicle data: Link based versus path based," *Transp. Res. Rec., J. Transp. Res. Board*, vol. 1768, pp. 157–161, Jan. 2001.
[23] D. Ettema and H. Timmermans, "Modeling departure time choice in the context of activity scheduling behavior," *Transp. Res. Rec., J. Transp. Res. Board*, vol. 1831, pp. 39–46, Jan. 2003.
[24] D. Ettema, F. Bastin, J. Polak, and O. Ashiru, "Modelling the joint choice of activity timing and duration," *Transp. Res. A, Policy Pract.*, vol. 41, no. 9, pp. 827–841, 2007.
[25] X. Zhang, G. Schildbach, D. Sturzenegger, and M. Morari, "Scenario-based MPC for energy-efficient building climate control under weather and occupancy uncertainty," in *Proc. Eur. Control Conf.*, Jul. 2013, pp. 1029–1034.
[26] S. Di Cairano, D. Bernardini, A. Bemporad, and I. V. Kolmanovsky, "Stochastic MPC with learning for driver-predictive vehicle control and its application to HEV energy management," *IEEE Trans. Control Syst. Technol.*, vol. 22, no. 3, pp. 1018–1031, May 2014.
[27] K. Liu *et al.*, "Comparison of very short-term load forecasting techniques," *IEEE Trans. Power Syst.*, vol. 11, no. 2, pp. 877–882, May 1996.
[28] J. W. Taylor and P. E. McSharry, "Short-term load forecasting methods: An evaluation based on European data," *IEEE Trans. Power Syst.*, vol. 22, no. 4, pp. 2213–2219, Nov. 2007.
[29] R. Huang, T. Huang, R. Gadh, and N. Li, "Solar generation prediction using the ARMA model in a laboratory-level micro-grid," in *Proc. IEEE SmartGridComm*, Nov. 2012, pp. 528–533.
[30] C. S. Ioakimidis, S. Lopez, K. N. Genikomsakis, P. Rycerski, and D. Simic, "Solar production forecasting based on irradiance forecasting using artificial neural networks," in *Proc. IEEE IECON*, Nov. 2013, pp. 8121–8126.
[31] A. Bemporad and M. Morari, "Control of systems integrating logic, dynamics, and constraints," *Automatica*, vol. 35, no. 3, pp. 407–427, Mar. 1999.
[32] H. Akaike, "Fitting autoregressive models for prediction," *Ann. Inst. Statist. Math.*, vol. 21, no. 1, pp. 243–247, 1969.
[33] T. L. Vandoorn, B. Meersman, L. Degroote, B. Renders, and L. Vandevelde, "A control strategy for islanded microgrids with DC-link voltage control," *IEEE Trans. Power Del.*, vol. 26, no. 2, pp. 703–713, Apr. 2011.
[34] K. Rouzbehi, A. Miranian, A. Luna, and P. Rodriguez, "DC voltage control and power sharing in multiterminal DC grids based on optimal DC power flow and voltage-droop strategy," *IEEE J. Emerg. Sel. Topics Power Electron.*, vol. 2, no. 4, pp. 1171–1180, Dec. 2014.
[35] COCN. (Mar. 2013). "Private commercialization for the urban and social infrastructure," (in Japanese), Council Competitiveness-Nippon, Tokyo, Japan, Annu. Rep., pp. 27–28. [Online]. Available: http://www.cocn.jp/thema55-L.pdf

Akira Ito (M'14) received the B.S. and M.S. degrees in engineering from Osaka Prefecture University, Sakai, Japan, in 1996 and 1998, respectively, and the Ph.D. degree in mechanical science and engineering from Nagoya University, Nagoya, Japan, in 2016, respectively.

In 1998, he joined DENSO CORPORATION, Kariya, Japan, where he is currently with the Department of Engineering Research and Development Center. His current research interests include control systems for advanced vehicles, advanced driver assistance systems, and energy management systems.

Dr. Ito is a member of The Society of Instrument and Control Engineers (SICE) and The Japan Society of Mechanical Engineers (JSME).

Akihiko Kawashima (M'14) was born in Chiba, Japan, in 1978. He received the Ph.D. degree in engineering from Chiba University, Chiba, in 2013.

He was a Post-Doctoral Researcher from 2013 to 2015, and he has been an Assistant Professor with Nagoya University, Nagoya, Japan. He has participated in a research project of the Core Research for Evolutional Science and Technology, Japan Science and Technology Agency, Tokyo, Japan. His current research interests include combinatorial optimization, computational complexity, and its application to the design of energy management systems.

Dr. Kawashima is a member of the SICE and the Institute of Electrical Engineers of Japan.

Tatsuya Suzuki (M'91) was born in Aichi, Japan, in 1964. He received the B.S., M.S., and Ph.D. degrees in electronic mechanical engineering from Nagoya University, Nagoya, Japan, in 1986, 1988, and 1991, respectively.

From 1998 to 1999, he was a Visiting Researcher with the Mechanical Engineering Department, University of California at Berkeley, Berkeley, CA, USA. He is currently a Professor with the Department of Mechanical Science and Engineering, Nagoya University, and a Principal Investigator with JST, CREST. His current research interests include intelligent mobility systems and the energy management systems.

Dr. Suzuki is a member of the SICE, The Institute of Systems, Control and Information Engineers, The Institute of Electronics, Information and Communication Engineers, The Society of Automotive Engineers of Japan (JSAE), The Robotics Society of Japan (RSJ), JSME, and Institute of Electrical Engineers of Japan (IEEJ). He received the best paper award in the International Conference on Advanced Mechatronic Systems 2013 and the outstanding paper award in the International Conference on Control Automation and Systems 2008. He also received the journal paper award from IEEJ, SICE, and JSAE in 1995, 2009, and 2010, respectively.

Shinkichi Inagaki (M'05) was born in Mie, Japan, in 1975. He received the B.S., M.S., and Ph.D. degrees in electronic mechanical engineering from Nagoya University, Nagoya, Japan, in 1998 and 2000, respectively, and the Ph.D. degree in precision engineering from The University of Tokyo, Tokyo, Japan, in 2003.

He was with Nagoya University as an Assistant Professor from 2003 to 2008 and a Lecturer from 2008 to 2015. He is currently an Associate Professor with the Department of Mechanical Science and Engineering, Nagoya University. His current research interests include energy management systems and decentralized control systems.

Dr. Inagaki is a member of the SICE, RSJ, and JSME.

Takuma Yamaguchi was born in Aichi, Japan, in 1986. He received the Ph.D. degree from the Department of Mechanical Science and Engineering, Nagoya University, Nagoya, Japan.

He is currently a Project Assistant Professor with Nagoya University. His current research interests include the design of driver assistance system, probabilistic fault diagnosis, energy management systems, and applications of model predictive control.

Dr. Yamaguchi is a member of the SICE.

Zhuomin Zhou received the B.S. degree in automobile engineering from Tsinghua University, Beijing, China, in 2006, and the M.S. and Ph.D. degrees in mechanical engineering from the University of Tsukuba, Tsukuba, Japan, in 2009 and 2012, respectively.

In 2013, he joined DENSO CORPORATION, Kariya, Japan, and currently with the Department of Engineering Research and Development Center. His current research interests include renewable energy systems, hydrogen systems, and energy management.

Dr. Zhou is a member of the Institute of Electrical Engineers of Japan.